

Temporal decomposition of EEG during a simple reaction time task into stimulus- and response-locked components

Yusuke Takeda, Kentaro Yamanaka, and Yoshiharu Yamamoto*

Educational Physiology Laboratory, Graduate School of Education, The University of Tokyo, 7-3-1 Hongo, Bunkyo-ku, Tokyo 113-0033, Japan

Received 15 March 2007; revised 3 August 2007; accepted 3 September 2007
Available online 14 September 2007

Brain activity during reaction time tasks has been reported to consist of stimulus- and response-locked components. The aim of this study is to apply a method for temporally extracting these components from human scalp electroencephalography (EEG) during an auditory simple reaction time task (SR-task). The stimulus- and response-locked components are extracted from each channel of the EEG epochs and reaction times (RTs) of all the trials by using a discrete Fourier transform; the performance of the method is verified using known simulation data. The extracted stimulus-/response-locked components are compared with the stimulus-/response-triggered average EEG during the SR-task, auditory-evoked potential (AEP) during the passive hearing of an auditory stimulus, and movement-related potential (MRP) during self-paced voluntary movement. For the EEG filtered with a bandpass of 1–40 Hz, the scalp distributions of negative peaks around 400 ms (N400) in the extracted stimulus-locked components are significantly different from those in the stimulus-triggered average EEG during the SR-task, suggesting that the late parts of the stimulus-triggered average EEG largely suffer from temporal smearing with the response-locked components. Furthermore, we show that the effect of the temporal smearing is large when slow waves remain in the EEG. In conclusion, these results confirm the feasibility and necessity of the decomposition method proposed.

© 2007 Elsevier Inc. All rights reserved.

Keywords: Simple reaction time; Evoked potentials; Decomposition; Stimulus-locked component; Response-locked component

Introduction

Brain activity during reaction time tasks has been reported to consist of stimulus-locked components and response-locked components (Braun et al., 2002; Endo et al., 1999; Goodin et al., 1986; Jung et al., 2001; Lamarre et al., 1983; Nelson, 1987; Nelson et al., 1991; Perfiliev, 1998; Tanji and Kurata, 1982). In human scalp electroencephalography (EEG) studies, these components are conventionally extracted by averaging EEG epochs with respect to either stimulus or response onset to increase the signal to noise

ratio. However, the conventional stimulus- or response-triggered average EEG does not reflect exactly pure stimulus- or response-locked brain activity, because these components are temporally overlapping especially in stimulus–response tasks with a short interval between stimulus and response onsets. In other words, the peak amplitudes and latencies of the conventional stimulus-/response-triggered average EEG are more or less affected by the temporal smearing. As a result, we cannot distinguish whether different waveforms of the stimulus-/response-triggered average EEG in different task conditions are attributable to the difference in the level of the temporal smearing due to a change in the reaction times (RTs) or to the difference in the stimulus-/response-locked EEG activity itself. Therefore, it is considered desirable to extract the pure stimulus- and response-locked components, not contaminated with each other, from EEG during reaction time tasks.

In this study, we propose a method temporally to decompose single-channel EEG data into stimulus- and response-locked components. In this method, these components are extracted from each channel of EEG epochs and RTs using a discrete Fourier transform, under the assumption that EEG data during a reaction time task consist of a stimulus-locked component, a response-locked component shifted by the RT of an individual trial, and noise. We apply this method to human surface EEG data during a simple reaction time task with an auditory stimulus (SR-task). To examine the effect of the temporal smearing by the averaging procedure, the extracted stimulus-/response-locked components are compared with the stimulus-/response-triggered average EEG during the simple reaction time task. Furthermore, we compare the extracted stimulus-locked component with an auditory-evoked potential (AEP) obtained by averaging the EEG during the passive hearing of an auditory stimulus, and also compare the response-locked component with a movement-related potential (MRP) obtained by averaging the EEG during self-paced voluntary movement.

Methods

Temporal decomposition of EEG

It is assumed that brain activity during a reaction time task consists of stimulus-locked activity, response-locked activity

* Corresponding author. Fax: +81 3 5689 8069.

E-mail address: yamamoto@p.u-tokyo.ac.jp (Y. Yamamoto).

Available online on ScienceDirect (www.sciencedirect.com).

shifted by the RT of an individual trial, and noise. Therefore, observed single-channel EEG data during a reaction time task can be expressed by:

$$y_n(t) = s(t) + r(t - \tau_n) + v_n(t) \quad t = 0, \dots, T - 1, \quad (1)$$

where $y_n(t)$: observed EEG data of trial n ; $s(t)$: stimulus-locked component; $r(t)$: response-locked component; τ_n : RT of trial n ; $v_n(t)$: noise of trial n . This implies that ongoing EEG activity and trial-to-trial variability of stimulus- and response-locked activity are included in $v_n(t)$.

By taking the discrete Fourier transform of Eq. (1), we obtain:

$$Y_n(\omega) = S(\omega) + \exp(-i2\pi\omega\tau_n/T)R(\omega) + V_n(\omega) \quad \omega = 0, \dots, T - 1, \quad (2)$$

where $Y_n(\omega)$ is the discrete Fourier transform of $y_n(t)$; $S(\omega)$ is the discrete Fourier transform of $s(t)$; $R(\omega)$ is the discrete Fourier transform of $r(t)$; $V_n(\omega)$ is the discrete Fourier transform of $v_n(t)$. Note that the last τ_n points in $r(t)$ should be zero, because the phase shift in the Fourier domain is equal to the circular shift in the time domain. By averaging Eq. (2) across n , we obtain:

$$\bar{Y}(\omega) = S(\omega) + \bar{E}(\omega)R(\omega) + \bar{V}(\omega), \quad (3)$$

where

$$\bar{Y}(\omega) = \frac{1}{N} \sum_{n=1}^N Y_n(\omega); \quad (4)$$

$$\bar{E}(\omega) = \frac{1}{N} \sum_{n=1}^N \exp(-i2\pi\omega\tau_n/T); \quad (5)$$

$$\bar{V}(\omega) = \frac{1}{N} \sum_{n=1}^N V_n(\omega), \quad (6)$$

and N is the total number of trials.

By solving Eqs. (2) and (3) simultaneously for $S(\omega)$ and $R(\omega)$, we obtain:

$$\frac{\exp(-i2\pi\omega\tau_n/T)\bar{Y}(\omega) - \bar{E}(\omega)Y_n(\omega)}{\exp(-i2\pi\omega\tau_n/T) - \bar{E}(\omega)} = S(\omega) + \frac{\exp(-i2\pi\omega\tau_n/T)\bar{V}(\omega) - \bar{E}(\omega)V_n(\omega)}{\exp(-i2\pi\omega\tau_n/T) - \bar{E}(\omega)}; \quad (7)$$

$$\frac{Y_n(\omega) - \bar{Y}(\omega)}{\exp(-i2\pi\omega\tau_n/T) - \bar{E}(\omega)} = R(\omega) + \frac{V_n(\omega) - \bar{V}(\omega)}{\exp(-i2\pi\omega\tau_n/T) - \bar{E}(\omega)}. \quad (8)$$

To prevent the denominators of Eqs. (7) and (8) from being zero, we use a function $D(n, \omega)$ instead of $\exp(-i2\pi\omega\tau_n/T) - \bar{E}(\omega)$,

$$D(n, \omega) = \begin{cases} c & \omega = 0 \\ \exp(-i2\pi\omega\tau_n/T) - \bar{E}(\omega) & \omega \neq 0 \end{cases}, \quad (9)$$

where c represents a constant number. By calculating Eq. (10) or (11) (see below) and from simulation results (not shown), we find that only the average of extracted components depends on the parameter c . So we can set c arbitrarily. In this study, we set c to unity.

Then, by averaging across n and taking the inverse discrete Fourier transform (IDFT), we obtain:

$$\begin{aligned} \text{IDFT} \left(\frac{1}{N} \sum_{n=1}^N \frac{\exp(-i2\pi\omega\tau_n/T)\bar{Y}(\omega) - \bar{E}(\omega)V_n(\omega)}{D(n, \omega)} \right) &= s(t) \\ + \text{IDFT} \left(\frac{1}{N} \sum_{n=1}^N \frac{\exp(-i2\pi\omega\tau_n/T)\bar{V}(\omega) - \bar{E}(\omega)V_n(\omega)}{D(n, \omega)} \right) &+ c_s; \end{aligned} \quad (10)$$

$$\begin{aligned} \text{IDFT} \left(\frac{1}{N} \sum_{n=1}^N \frac{Y_n(\omega) - \bar{Y}(\omega)}{D(n, \omega)} \right) \\ = r(t) + \text{IDFT} \left(\frac{1}{N} \sum_{n=1}^N \frac{V_n(\omega) - \bar{V}(\omega)}{D(n, \omega)} \right) + c_r, \end{aligned} \quad (11)$$

where c_s and c_r represent the shifts of the averages by $D(n, \omega)$.

Eqs. (10) and (11) show that $s(t)$ or $r(t)$ plus a noise term can be obtained by calculating the left-hand side of Eq. (10) or (11). The noise terms converge to zero as N increases, because the average of $V_n(\omega)$ converges to zero as N increases, whereas $D(n, \omega)$ varies depending on τ_n regardless of N . Let us refer to the real parts of the left-hand sides of Eqs. (10) and (11) as the extracted stimulus-locked component and the extracted response-locked component, respectively.

Before applying the decomposition method, we need to set the parameters l_0 , the number of data points before stimulus and response onset, and l_1 , the number of data points after stimulus and response onset. We need to set l_1 to be adequately long so that the last data points in $r(t)$, which must be longer than the maximum τ_n , will be the baseline. In this study, we set l_0 to 100 and l_1 to 300, which correspond with 500 ms and 1500 ms, respectively, if the sampling rate is 200 Hz.

The Matlab codes for this decomposition method are available at: “www.p.u-tokyo.ac.jp/~takeda/decomp/”.

Simulation with artificial data

In order to verify the performance of the decomposition method, a numerical experiment was performed on a set of known signals. In this simulation, the original stimulus- and response-locked components were generated by the exponential and the cosine functions, respectively. The RTs, which were randomly selected from actual RTs of all the subjects (as described in the Data analyses subsection), were used as τ_n ($n=1, \dots, N=100$), and white noise [standard deviation (SD)=0.5] was used as $v_n(t)$ (Fig. 1A). The simulated signal $y_n(t)$ was generated from $s(t)$, $r(t)$, τ_n and $v_n(t)$ according to Eq. (1) (Fig. 1B). Then, we extracted the stimulus- and response-locked component by Eqs. (10) and (11), respectively. The similarity of the extracted and original components was quantified by calculating the correlation coefficient between these two waveforms.

Further, to evaluate the residual errors between the extracted and original stimulus-/response-locked components, we repeated the above procedure 500 times using different sets of white noise and τ_n . The averages of the residual errors across time were adjusted to zero. To examine whether the residual errors fluctuate randomly around zero, the time courses of the mean and SD of the 500 residual errors were plotted (Figs. 2B1, C1). To examine the

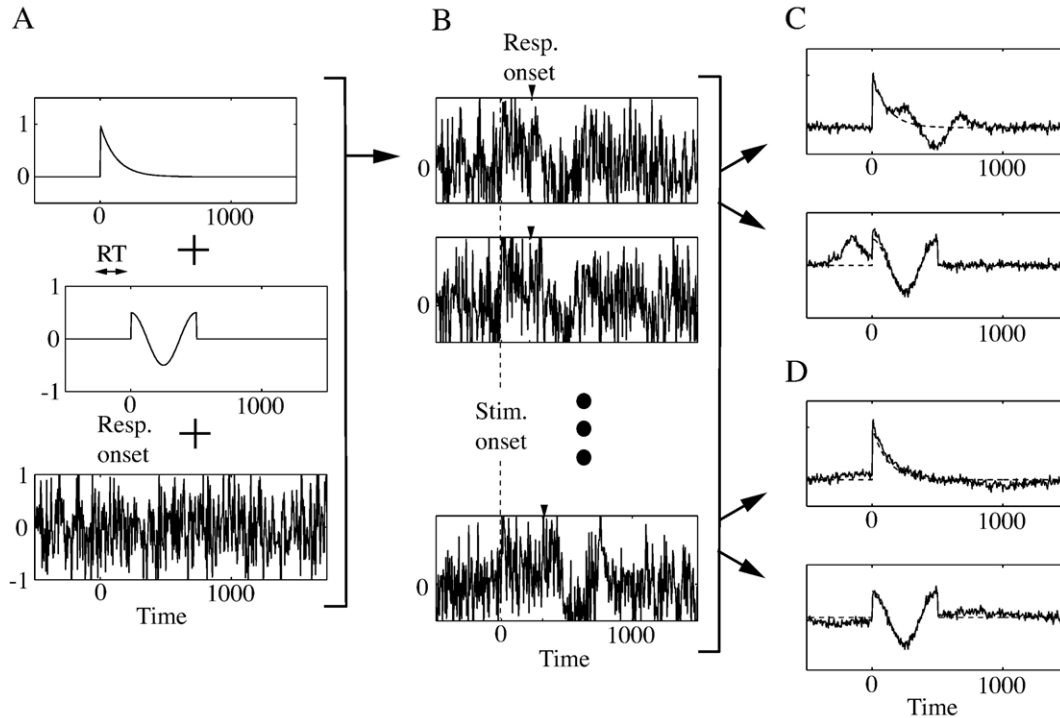


Fig. 1. Simulations with artificial data. (A) The original stimulus-locked component (top), response-locked component (middle), and noise (bottom). (B) The simulated data obtained by Eq. (1) and the RTs from which the stimulus- and response-locked components are extracted. (C) The stimulus-triggered average of the simulated data (solid line) and the original stimulus-locked component (dotted line) (top); the response-triggered average of the simulated data (solid line) and the original response-locked component (dotted line) (bottom). The effects of temporal smearing are observed in the late part of the stimulus-triggered average and in the early part of the response-triggered average. (D) The extracted (solid line) and original (dotted line) stimulus-locked component (top); the extracted (solid line) and original (dotted line) response-locked component (bottom).

frequency characteristics of the residual errors (Figs. 2B1, C1), we calculated the amplitude spectrum (Figs. 2B2, C2):

$$AP(\omega) = \frac{1}{500} \sum_{p=1}^{500} |RE_p(\omega)|, \quad (12)$$

where $RE_p(\omega)$ represents the Fourier transform of the p -th residual error re_p of the 500 repetitions. Finally, we examined how the noise level in the extracted stimulus-/response-locked components decreased as the number of trials increased (Figs. 2B3, C3). The noise level $NL(N)$ was obtained by calculating the variance of the residual error as follows:

$$NL(N) = \frac{1}{500} \sum_{p=1}^{500} \left[\frac{1}{T-1} \sum_{t=0}^{T-1} re_{p,N}(t)^2 \right], \quad (13)$$

where $re_{p,N}(t)$ represents the p -th residual error obtained from the simulation data consisting of N trials. The variance was fitted by a function $y=a/x$ by the least square method. Further, in order to compare the noise level in the component obtained by our method with that by the averaging procedure, the noise used in the above repeated simulations was simply averaged across trials, and examined in the same manner as the residual errors (Figs. 2A1–3).

Simulation with EEG data

In order to test the performance of the method for more EEG-like data, an additional numerical experiment was performed

using real EEG data (Fig. 3). In this simulation, the AEP and MRP (described in the Data analyses subsection) were used as the original stimulus- and response-locked components, respectively, and the RTs, which were randomly selected from RTs of all the subjects, were used as τ_n ($n=1, \dots, N=400$). The EEG data related to neither the stimulus nor the response were used as the noise; we randomly selected them from EEG in the interval of 2500–500 ms before the stimulus onset during the SR-tasks of all the subjects (described in the Experimental procedures subsection). As the simulation with the artificial data suggested the need to apply a high-pass filter before decomposing real EEG involving non-negligible slow waves (see the Results section), we applied three kinds of filters to the noise EEG data: no filtering, bandpass of 1–40 Hz and bandpass of 2–40 Hz (described in the Data analyses subsection). By using the AEP, MRP, RTs and noise EEG data, we generated the simulated EEG data according to Eq. (1).

Then, we extracted the stimulus- and response-locked components from the simulated EEG data (Figs. 3A–C1, A–C2). To examine the residual errors between the extracted and original components, we repeated the above procedure 100 times using different sets of the noise and τ_n . The averages of the residual errors across time were adjusted to zero. To examine whether the residual errors fluctuate randomly around zero, the time course of the mean and SD of the residual errors across the repeated procedures were plotted (Figs. 3A–C3). Then, we examined how the noise level decreased as the number of trials N increased (Figs. 3A–C4, diamond). The noise level $NL(N)$ was

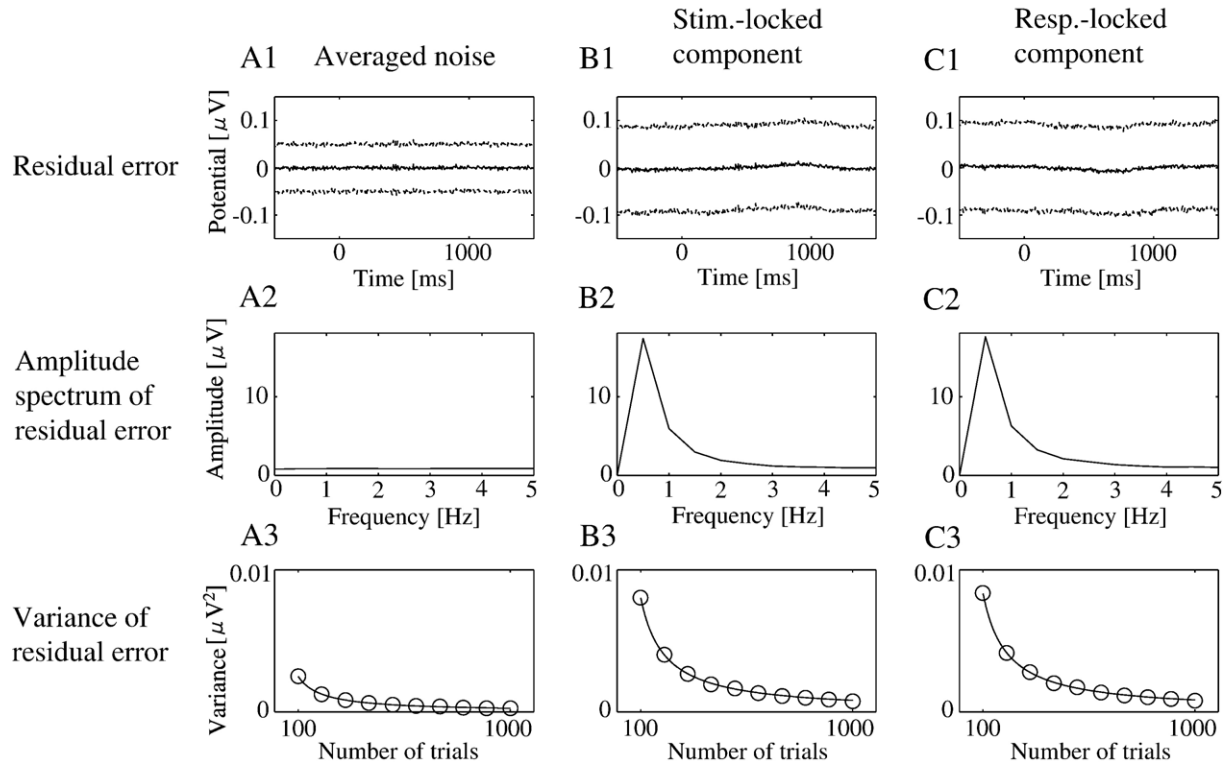


Fig. 2. Residual errors between the original and extracted stimulus-/response-locked components for simulated artificial data. (A1–C1) Means (solid lines) and means \pm SD (dotted lines) of the averaged noise (A1) and of the residual errors across 500 repeated simulations as in Fig. 1 (B1, C1). (A2–C2) Amplitude spectra of the averaged noise (A2) and of the residual errors (B2, C2). (A3–C3) Variance of the averaged noise (A3) and of the residual errors (B3, C3) as a function of the total number of trials N (circle). Solid lines represent fitting curves in the form of $y = a/x$. (A1–A3) Results for the averaged noise across trials. (B1–B3) Results for the residual errors for the extracted stimulus-locked component. (C1–C3) Results for the residual errors for the extracted response-locked component.

obtained by calculating the variance of the residual errors as follows:

$$NL(N) = \frac{1}{100 \times 2} \sum_{p=1}^{100} \left[\frac{1}{T-1} \sum_{t=0}^{T-1} \text{re}_{p,N,s}(t)^2 + \frac{1}{T-1} \sum_{t=0}^{T-1} \text{re}_{p,N,r}(t)^2 \right], \quad (14)$$

where $\text{re}_{p,N,s}(t)$ and $\text{re}_{p,N,r}(t)$, respectively, represent the p -th residual errors of the extracted stimulus- and response-locked components obtained from the simulation data consisting of N trials. The variance was fitted by a function $y = a/x$ by the least square method. Further, in order to compare the noise level in the components extracted by our method with that obtained by the averaging procedure, the noise EEG data used in the above repeated simulations were simply averaged across trials, and examined in the same manner as the residual errors (Figs. 3A 4–C4, circle).

By comparing the parameter a of the fitting function of the extracted components with that of the averaged noise, we were able to estimate the number of trials our method needs in order to achieve the same noise level as the averaging procedure. Let us refer to the coefficient a obtained from the extracted component as a_c , and that obtained from the averaged noise as a_n . The equality of the variance of the residual errors to that of the averaged noise leads to the following equation:

$$a_c/x_c = a_n/x_n, \quad (15)$$

where x_c and x_n represent the number of trials used for the decomposition and the averaging, respectively. Eq. (15) can be rewritten as:

$$a_c/a_n = x_c/x_n. \quad (16)$$

Eq. (16) means that the decomposition method requires a_c/a_n times as many trials as the averaging procedure in order to achieve the same noise level.

Experimental procedures

Thirteen healthy adults aged between 20 and 31 years old constituted the experimental population. All the subjects gave their informed consent, and the local ethics committee approved the experimental procedure.

The subjects were seated comfortably in a chair with their eyes closed and right index finger placed on a button. The behavioral experiment consisted of 6 sessions. In each of the sessions, the subjects were instructed to perform three kinds of tasks in the following order: a simple reaction time task (SR-task), a stimulus task (S-task) and a movement task (M-task). In the SR-task, the subjects were instructed to press the button as soon as possible after hearing an auditory stimulus (75 dB SPL, 2 ms duration, 3500 Hz). The auditory stimulus was presented via earphones. The inter-stimulus interval was randomized from 4 to 7 s. In the S-task, the subjects were instructed passively to hear the same auditory stimulus. The inter-stimulus interval was randomized from 2 to 3 s.

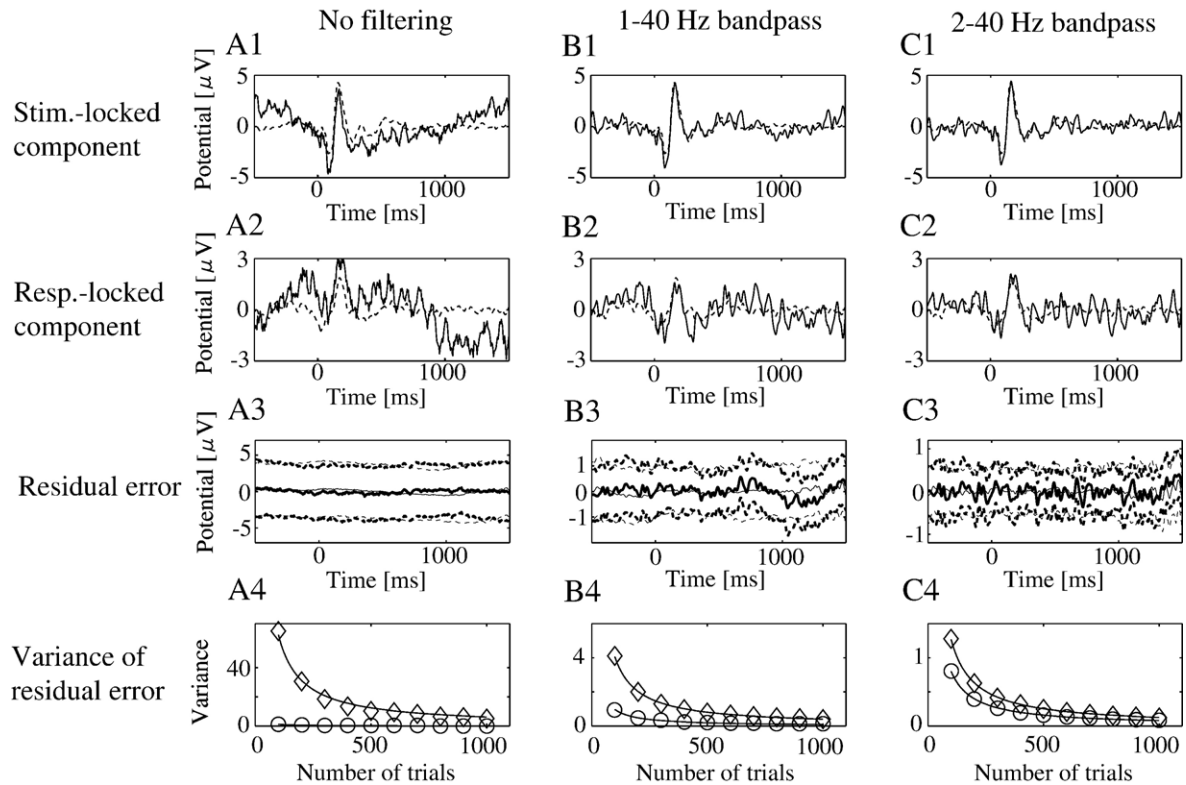


Fig. 3. Simulations with EEG data. (A1–C1) Extracted stimulus-locked components (solid lines) and the original AEP data used for the simulation (dotted lines). (A2–C2) Extracted response-locked components (solid lines) and the original MRP data used for the simulation (dotted lines). (A3–C3) Residual errors between the extracted and original stimulus-/response-locked components. Thick and thin solid lines represent the means of the residual errors across the repeated simulations for the stimulus- and response-locked components, respectively. The thick and thin dotted lines represent the means \pm SD of the residual errors across the repeated simulations for the stimulus- and response-locked components, respectively. (A4–C4) Variance of the residual errors between the extracted and original components (diamond) and that of the averaged noise across trials (circle) as a function of the total number of trials N . Solid lines represent fitting curves in the form of $y = a/x$. (A1–A4) Result for the simulations in which pre-stimulus EEG without filtering was used as the noise. (B1–B4) Result for the simulations in which pre-stimulus EEG filtered with 1–40 Hz was used as the noise. (C1–C4) Result for the simulations in which pre-stimulus EEG filtered with 2–40 Hz was used as the noise.

In the M-task, the subjects were instructed to press the button repeatedly at an interval of about 4 s in the same manner as the SR-task. In total, about 300 trials were collected for each task from each of the subjects.

During the tasks, surface EEG was recorded from 19-ch electrodes located according to the International 10–20 System. The EEG was amplified on a Nihon Kohden EEG-1100 with a time constant of 0.3 s. Because we expected that large EEG activity related to the task execution would not appear around the earlobes, we placed reference electrodes on both earlobes and recorded their potentials separately. Their averaged potentials were subtracted from the EEG data offline. For monitoring eye movements, an electrooculography (EOG) was recorded with a pair of electrodes placed above and below the left eye. The sampling rate of the EEG and the EOG was 1000 Hz.

Data analyses

In an offline analysis, we resampled the EEG data at the rate of 200 Hz. The simulation results (Figs. 2 and 3) gave rise to the need to reduce slow waves in the EEG by a digital filter before the decomposition (see the Results section). Therefore, the EEG data was filtered with the bandpass of 1–40 Hz and of 2–40 Hz by using

three kinds of finite impulse (FIR) filters: the high-pass of 1 Hz (600-point, -20 dB at 0.5 Hz), the high-pass of 2 Hz (300-point, -26 dB at 1 Hz) and the low-pass of 40 Hz (15-point, -45 dB at 50 Hz). Then, we segmented the filtered EEG data into 2-s epochs from -500 to 1500 ms after the stimulus onset for the SR- and S-task, or after the button push onset for the M-task.

Reaction times were defined as the intervals between the stimulus onset and the button push signal onset. In the following analysis, we used the 19-ch EEG epochs of the trials in which RTs were within 100–400 ms and EOG were within ± 100 μ V. In addition, an artifact criterion of ± 100 μ V was used for each of the channels to reject trials with excess electromyographic activity or measurement noise. Because huge measurement noise was included in one subject's EEG data, we excluded his/her data from the analysis.

The stimulus- and response-locked components were obtained by Eqs. (10) and (11), respectively, from each set of the EEG epochs and the RTs during the SR-task. The extracted stimulus-locked components were then compared with the stimulus-triggered average EEG during the SR-task and with the AEP obtained by averaging the EEG epochs during the S-task triggering the stimulus onset. We set the baseline at the interval from 100 to 0 ms before the stimulus onset, and subtracted the average potentials during the

interval from these three potentials for individual channels. The extracted response-locked components were compared with the response-triggered average EEG during the SR-task and with the MRP obtained by averaging the EEG epochs during the M-task triggering the response onset. We set the baseline at the interval from 500 to 400 ms before the response onset, and subtracted the average potentials during the interval from these three potentials for individual channels.

In the extracted stimulus-locked components (Fig. 4A), negative peaks around 100 ms (N100), positive peaks around 160 ms (P200), positive peaks around 315 ms (P300) and negative peaks around 410 ms (N400) were observed. In the extracted response-locked components (Fig. 4B), negative peaks around -40 ms (N-40), positive peaks around 160 ms (P160) and negative peaks around 500 ms (N500) were observed. Since we expected that the effects of the temporal smearing would be large in the late parts of the stimulus-triggered average EEG and in the early parts of the response-triggered average EEG (see Fig. 1C), in this study, we only examined the scalp distributions of the P300, N400, N-40 and P160. Indeed, we confirmed that peak amplitudes, latencies, and scalp distributions of the other potentials earlier than the P300 or later than the P160 were not substantially different depending on the methods used (not shown).

For the stimulus-locked component and the stimulus-triggered average EEG during the SR-task, the peak latencies of the P300 and N400 were measured from the extracted stimulus-locked components at Cz as the time points of the largest positive and negative peaks within 250–350 and 300–500 ms. For the AEP, its peak latencies were measured from the AEP at Cz in the same manner. For the response-locked component and the response-triggered average EEG during the SR-task, the peak latencies of the N-40 and P160 were measured from the extracted response-locked components at Cz as the time points of the largest negative and positive peaks within -100 – 100 and 50–250 ms. For the MRP, its peak latencies were measured from the MRP at Cz in the same manner. Then, scalp distributions were obtained from the 19-ch potentials at these latencies and compared with each other.

To confirm that the differences of the scalp distributions between the extracted stimulus-/response-locked components and the conventional stimulus-/response-triggered average EEG during the SR-task are attributable to the temporal overlapping with each other, we reconstructed stimulus-/response-triggered average EEG

by overlapping both of the extracted stimulus- and response-locked components with the delays of the individual RTs according to Eq. (1).

The similarities of the scalp distributions by different methods were quantified by a dot product (dp). We normalized the 19-dimensional EEG vectors to unit vectors with a magnitude of 1, and calculated a dot product between the vectors, where the dot product of 1 represents perfect similarity of the distributions. A two-tailed Wilcoxon signed-rank test was conducted to test the null hypothesis that the dot products obtained from each of the subjects did not differ from zero. Also, peak amplitudes in different waveforms were compared by means of the two-tailed Wilcoxon signed-rank test. In this study, an α level of 0.05 was used for the statistical test.

Results

Simulation with artificial data

We extracted the original components used for the simulation with the artificial data from the simulated signals (Fig. 1). The extracted and original stimulus-locked components are highly correlated [$r_s=0.93$ (r_s : the correlation coefficient between the extracted and original stimulus-locked components)], as are the extracted and original response-locked components [$r_r=0.90$ (r_r : the correlation coefficient between the extracted and original response-locked components)] (Fig. 1D).

Fig. 2 shows the detailed property of the residual errors between the extracted and original components. The time courses of the mean and SD of the residual errors are almost constant (Figs. 2B1, C1), indicating that the residual errors have no temporal modulation patterns and fluctuate randomly. Note that the SD of the residual errors [0.091 ± 0.0025 (mean \pm SD)] is larger than that of the averaged noise (0.050 ± 0.0016), indicating that the noise level of the components extracted by our method is larger than that obtained by the averaging procedure. The large amplitude spectra of the residual errors at low frequencies (Figs. 2B2, C2) indicate that the larger residual errors are attributable to amplified slow waves in the noise. The variance of the residual errors is inversely proportional to the number of trials N , in the same way as the averaged noise (Figs. 2A–C3), indicating that the noise level of the extracted components decreases as the number of trials increases. The coefficient is $a_n=0.25$ for the averaged noise, while $a_c=0.80$ for the

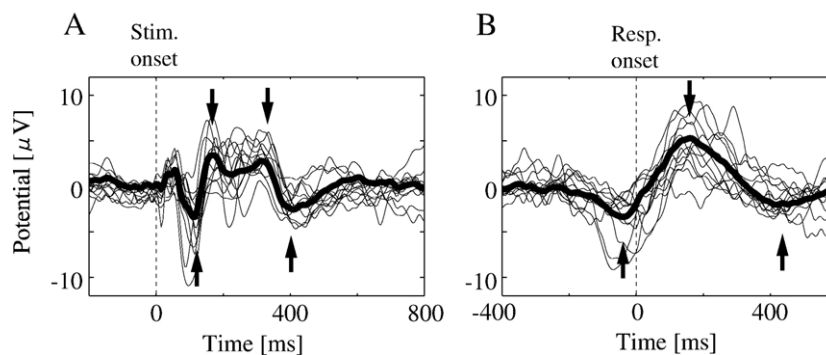


Fig. 4. Extracted stimulus- and response-locked components at Cz. (A) Extracted stimulus-locked components. Arrows indicate, from left to right, the N100, P200, P300 and N400. (B) Extracted response-locked components. Arrows indicate, from left to right, the N-40, P160 and N500. Thick lines represent the components extracted from all the subjects' EEG and RTs; thin lines represent the components extracted for each subject. In this figure, the average of each wave is adjusted to zero.

extracted stimulus-locked component and $a_c=0.83$ for the extracted response-locked component. Thus, the ratios a_c/a_n in Eq. (16) are 3.2 and 3.3 for the stimulus- and response-locked components, respectively. This indicates that our decomposition method needs about 3.3 times as many trials as the averaging procedure in order to achieve the same noise level, when the noise is white.

Simulation with EEG data

We also extracted the original stimulus-/response-locked components used for the simulation with the EEG data from the simulated signals (Fig. 3). Baseline fluctuations of the components extracted from the simulated EEG without filtering are large (Figs. 3A1, A2), whereas those obtained from the filtered EEG are well suppressed (Figs. 3B1, B2, C1, C2). Indeed, the correlation coefficient between the extracted and original components is low for the EEG without filtering ($r_s=0.52$, $r_r=0.30$), whereas it is much higher for the filtered EEG ($r_s=0.79$, $r_r=0.51$ for the EEG filtered with 1–40 Hz; $r_s=0.85$, $r_r=0.54$ for the EEG filtered with 2–40 Hz). This is because the remaining slow waves in the EEG without filtering are amplified by the decomposition. The time courses of the mean and SD of the residual errors are almost constant, indicating that the residual errors have no temporal modulation patterns and fluctuate randomly regardless of the filter properties.

The variance of the residual errors is inversely proportional to the number of trials, in the same way as the averaged noise (Figs. 3A–C4), but the coefficients a_c for the extracted components are consistently greater than the a_n for the averaged noise. These coefficients are presented in Table 1, and it is shown that our decomposition method needs 1.6 times as many trials as the averaging procedure in order to achieve the same noise level when slow waves in the EEG lower than 2 Hz are eliminated.

Decomposition of observed EEG (1–40 Hz)

We obtained 256.8 ± 34.7 trials per subject for the SR-task. The mean and SD of all the RTs are 221.0 ms and 57.8 ms, respectively. We first decomposed the EEG filtered with 1–40 Hz during the SR-task. Fig. 4 shows the stimulus and responses-locked components extracted from each/all of the subjects' EEG at Cz, and the RTs. The extracted stimulus-locked component at Cz exhibits the N100, P200, P300 and N400 (Fig. 4A). The extracted response-locked component at Cz exhibits the N-40, P160 and N500 (Fig. 4B).

Extracted stimulus-locked component

Fig. 5 shows the extracted stimulus-locked components, the stimulus-triggered average EEG during the SR-task and the AEP obtained from all the subjects' EEG data. The AEP was obtained

Table 1
Coefficients a of a fitting function $y=a/x$ for an error level y as a function of the number of trials x

	EEG (no filter)	EEG (1–40 Hz)	EEG (2–40 Hz)
a_c	6241	407	127
a_n	125	98	80
a_c/a_n	50	4.2	1.6

a_c : Coefficients obtained from the components extracted by our method.

a_n : Coefficients obtained from the averaged noise.

from 269.8 ± 36.4 trials per subject during the S-task. Fig. 7A shows the scalp distributions of the P300 and N400 in each of the waveforms.

At around the P300, the waveforms of the extracted stimulus-locked components shift frontally as compared to those of the stimulus-triggered average EEG during the SR-task; the amplitudes of the P300 in the extracted stimulus-locked components are large at around Fp1 and Fp2, whereas those in the stimulus-triggered average EEG during the SR-task are large at around Cz (Fig. 5). However, the dp of the P300 between both waves are significantly greater than zero ($dp=0.74 \pm 0.26$, $p < 0.05$) (Fig. 7A). This result indicates that the differences between the extracted stimulus-locked component and the stimulus-triggered average EEG appear to exist at around the P300, but is not reflected in the (global) dp measure.

In the AEP, clear P300 waveforms are not observed (Fig. 5), although the dp of the P300 between the AEP and the extracted stimulus-locked components are significantly greater than zero ($dp=0.69 \pm 0.22$, $p < 0.05$) (Fig. 7A).

At around the N400, the waveforms of the extracted stimulus-locked components are clearly different from those of the stimulus-triggered average EEG during the SR-task; the amplitudes of the N400 in the extracted stimulus-locked components are large at around Cz, whereas those in the stimulus-triggered average EEG during the SR-task are large at around Fp1 and Fp2 (Fig. 5). The dp of the N400 between both waves are not significantly greater than zero ($dp=0.13 \pm 0.38$, $p > 0.05$) (Fig. 7A). It is of note that the amplitudes of the N400 in the reconstructed stimulus-triggered average EEG are large at around Fp1 and Fp2, in the same way as the observed stimulus-triggered average EEG, and the dp between them approach 1.0 ($dp > 0.99$ for all the subjects) (Fig. 7A). This result indicates that the differences in the N400 amplitudes between the extracted stimulus-locked components and the stimulus-triggered average EEG disappear by overlapping the extracted response-locked components on the extracted stimulus-locked components, suggesting that the differences are attributable to the overlap of the response-locked components.

In the AEP, the amplitudes of the N400 are large at around Cz, as are those in the extracted stimulus-locked components (Fig. 5), and the dp of the N400 between them are significantly greater than zero ($dp=0.37 \pm 0.44$, $p < 0.05$) (Fig. 7A).

Extracted response-locked component

Fig. 6 shows the extracted response-locked components, the response-triggered average EEG during the SR-task and the MRP obtained from all the subjects' EEG data. The MRP was obtained from 236.8 ± 32.3 trials per subject during the M-task. Fig. 7B shows the scalp distributions of the N-40 and P160 in each of the waveforms.

The amplitudes of the N-40 in the extracted response-locked components are large at around Cz, as is the response-triggered average EEG during the SR-task (Fig. 6), and the dp of the N-40 between both waves are significantly greater than zero ($dp=0.72 \pm 0.18$, $p < 0.05$) (Fig. 7B).

In the MRP, clear N-40 waveforms are not observed, in contrast to the extracted response-locked component (Fig. 6), although the dp of the N-40 between them are significantly greater than zero ($dp=0.54 \pm 0.43$, $p < 0.05$) (Fig. 7B).

The amplitudes of the P160 in the extracted response-locked components are large at around Cz, as is the response-triggered average EEG during the SR-task (Fig. 6), and the dp of the P160

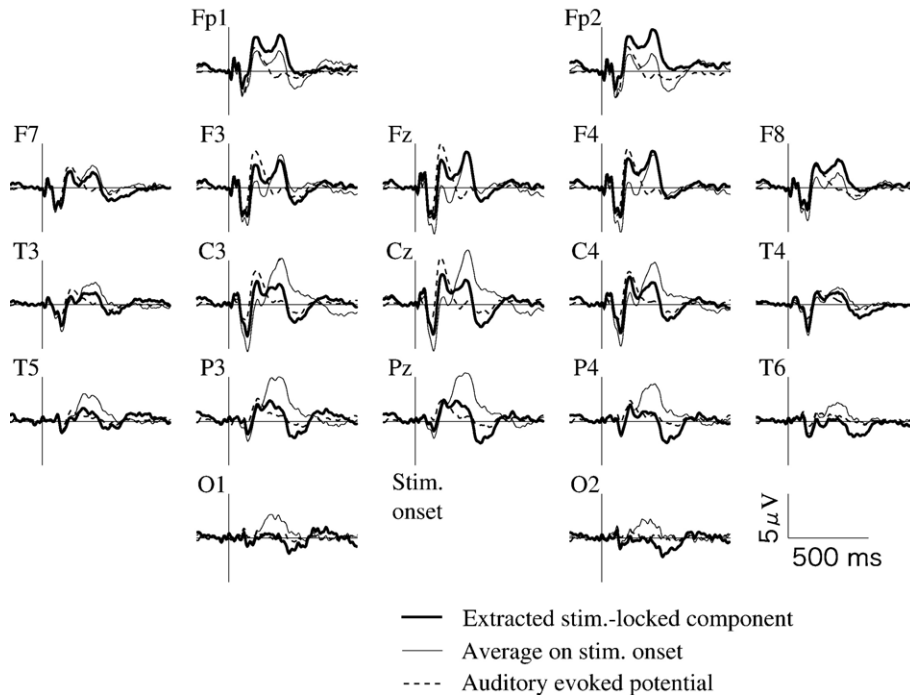


Fig. 5. Extracted stimulus-locked components, stimulus-triggered average EEG during the SR-task and the AEP obtained from all the subjects' EEG.

between both waves are significantly greater than zero ($dp=0.75 \pm 0.20$, $p < 0.05$) (Fig. 7B).

In the MRP, the amplitudes of the P160 are large at around Cz, as are those in the extracted response-locked components (Fig. 6), and the dp of the P160 between them are significantly greater than zero ($dp=0.60 \pm 0.41$, $p < 0.05$) (Fig. 7B).

On the other hand, the N-40 and P160 amplitudes of the extracted response-locked components do not exhibit significant differences between C3 and C4 (-4.1 ± 4.6 and -4.0 ± 3.4 , respectively, $p > 0.05$ for the N-40; 4.8 ± 2.5 and 3.5 ± 2.8 , respectively, $p > 0.05$ for the P160), although the response-triggered average EEG does exhibit significant differences (-4.4 ± 2.4 and -3.7 ± 1.9 ,

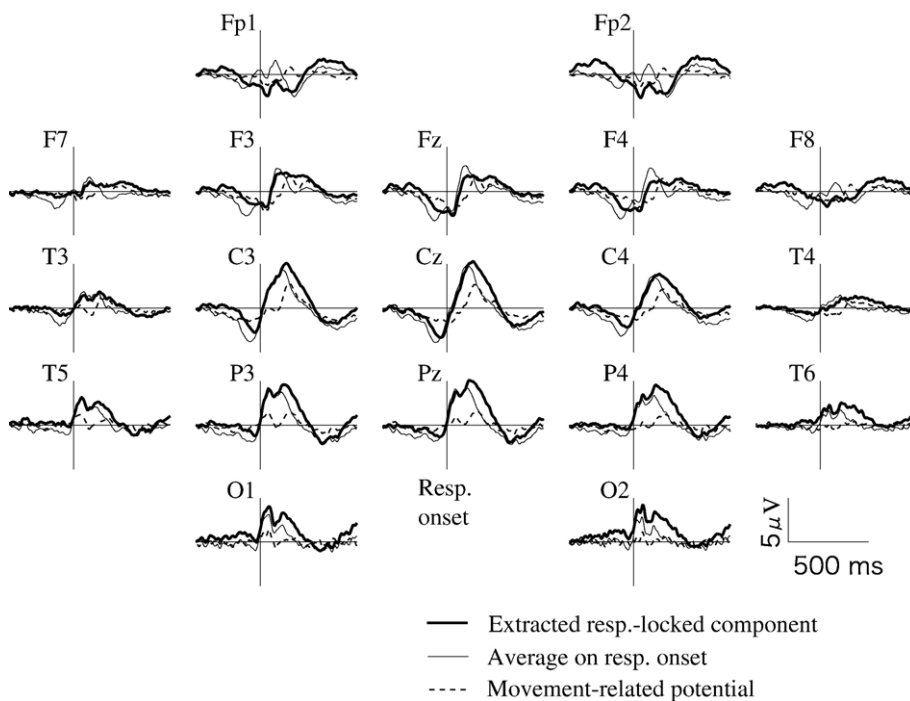


Fig. 6. Extracted response-locked components, response-triggered average EEG during the SR-task and the MRP obtained from all the subjects' EEG.

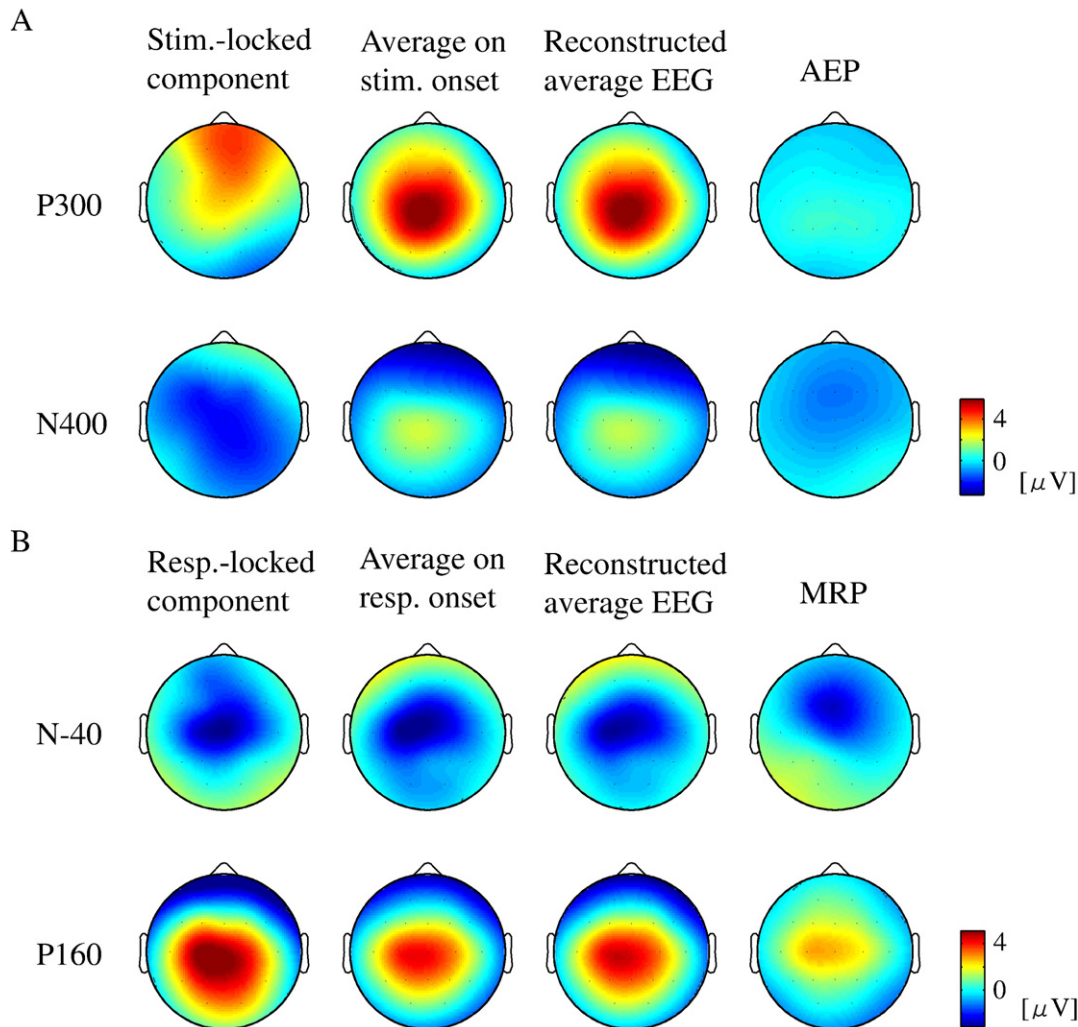


Fig. 7. Scalp distributions of the P300, N400, N-40 and P160. (A) The P300 and N400 in the extracted stimulus-locked components, the stimulus-triggered average EEG, the reconstructed stimulus-triggered average EEG and the AEP obtained from all the subjects' EEG. (B) The N-40 and P160 in the extracted response-locked components, the response-triggered average EEG, the reconstructed response-triggered average EEG and the MRP obtained from all the subjects' EEG.

respectively, $p < 0.05$ for the N-40; 5.1 ± 2.2 and 4.2 ± 1.9 , respectively, $p < 0.05$ for the P160).

Decomposition of observed EEG (2–40 Hz)

We also decomposed the EEG filtered with 2–40 Hz during the SR-task. Fig. 8 shows the extracted stimulus-/response-locked components and the stimulus-/response-triggered average EEG during the SR-task obtained from all the subjects' data.

The extracted stimulus-locked component at Cz exhibits the P300 and N400 in the same way as that extracted from the EEG filtered with 1–40 Hz (Fig. 8A). In contrast to the EEG filtered with 1–40 Hz, however, the stimulus-triggered average EEG at Cz has the P300 and N400 peaks in the same way as the extracted stimulus-locked component (Fig. 8A). The amplitudes of the P300 and N400 in the stimulus-triggered average EEG are large at around Fz in the same way as the extracted stimulus-locked components (Fig. 8B), and the dp of the P300 and N400 between them are significantly greater than zero ($dp = 0.91 \pm 0.14$, $p < 0.05$ for the P300; $dp = 0.91 \pm$

0.12 , $p < 0.05$ for the N400). These results indicate that, in the case of the EEG filtered with 2–40 Hz, the effect of the temporal smearing by the response-locked components is not so large as to change these scalp distributions significantly.

Similar to the EEG filtered with 1–40 Hz, both the extracted response-locked component and the response-triggered average EEG at Cz exhibit the N-40 and P160 (Fig. 8C). The amplitudes of the N-40 and P160 in the response-triggered average EEG are large at around Cz in the same way as the extracted response-locked components (Fig. 8D), and the dp of the N-40 and P160 between them are significantly greater than zero ($dp = 0.87 \pm 0.11$, $p < 0.05$ for the N-40; $dp = 0.92 \pm 0.067$, $p < 0.05$ for the P160). On the other hand, the amplitudes of the N-40 and P160 at Cz in the response-locked components are significantly smaller than those in the response-locked components extracted from the EEG filtered with 1–40 Hz (-2.63 ± 1.07 and -4.82 ± 3.44 , respectively, $p < 0.05$ for the N-40; 4.03 ± 1.07 and 5.31 ± 2.27 , respectively, $p < 0.05$ for the P160). This result suggests that the above-mentioned small effect of the temporal smearing by the response-

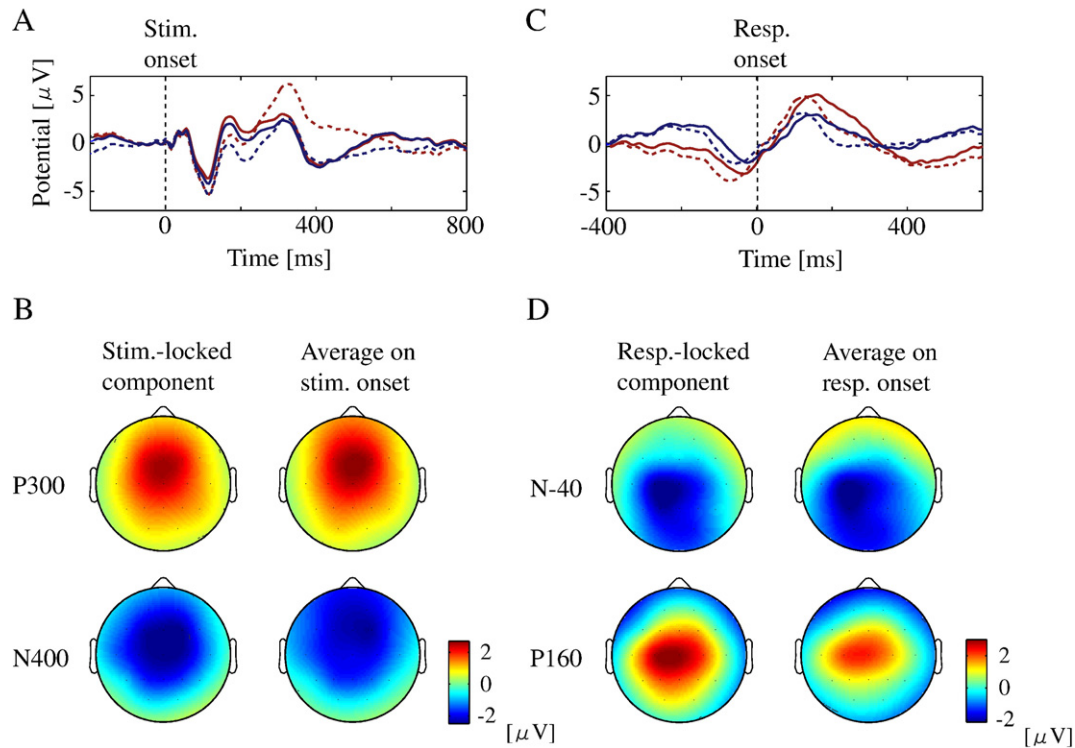


Fig. 8. Decomposition of EEG (2–40 Hz) during the SR-task. (A) Extracted stimulus-locked component at Cz (blue solid line) and stimulus-triggered average EEG during the SR-task at Cz (blue dotted line). For comparison, the stimulus-locked component at Cz and the stimulus-triggered average EEG at Cz obtained from the EEG filtered with 1–40 Hz are superimposed (red solid and red dotted lines, respectively). (B) Scalp distributions of the P300 and N400 in the extracted stimulus-locked components and the stimulus-triggered average EEG during the SR-task. (C) Extracted response-locked component at Cz (blue solid line) and response-triggered average EEG during the SR-task at Cz (blue dotted line). For comparison, the response-locked component at Cz and the response-triggered average EEG at Cz obtained from the EEG filtered with 1–40 Hz are superimposed (red solid and red dotted lines, respectively). (D) Scalp distributions of the N-40 and P160 in the extracted response-locked components and the response-triggered average EEG during the SR-task.

locked components is due to the attenuated peaks in the response-locked components.

Discussion

In this study, we propose a method for extracting stimulus- and response-locked components from single-channel EEG data. The performance of the algorithm is examined by two types of simulation tests. Then, we apply the method to 19-ch EEG data during the SR-task, and compare the extracted stimulus-/response-locked components with the stimulus-/response-triggered average EEG during the SR-task. As a result, it is shown that the late parts of the stimulus triggered average EEG are largely smeared by the overlap of the response-locked components in the case of the EEG filtered with 1–40 Hz.

Methodological considerations

In the proposed method, we assume that the EEG during reaction time tasks consist of the stimulus-locked component, the response-locked component shifted by the RT of an individual trial, and noise. An alternative assumption would be that the stimulus-locked component is followed by the response-locked component without overlapping, in which the stimulus and/or response-locked components are expanded/compressed with RT. Since some studies are implicitly based on this assumption (Gibbons and Stahl, 2007; Thompson et al., 1996), we examine whether the assumption is also

valid for the EEG during the SR-task by comparing the stimulus-triggered average EEG of fast responses with that of slow responses; under the assumption, the peak latencies should vary depending on the RTs. As a result (not shown), the latencies of the N100 and P200 are almost the same regardless of the RTs, and this result is in agreement with other previous reports (Falkenstein et al., 1993; Hohnsbein et al., 1991). Therefore, we consider this assumption not to be suitable, at least for the EEG during simple reaction time tasks.

Then, we adopt the assumption of this study, which is that the stimulus- and response-locked components are overlapping and the delay of the response-locked component is somehow responsible for the variability of the RTs. However, it is not appropriate additionally to assume that the waveforms of the stimulus- and response-locked components are constant or independent of each other, because, in some cases, peak amplitudes or latencies in the components may vary more or less with RTs (Mihaylova et al., 1999; Vassilev et al., 2002; Vaughan et al., 1966). Note that $s(t)$ and $r(t)$ in Eq. (1) represent the average waveforms of the stimulus- and response-locked components, and that trial-to-trial variability of these components is included in the noise term of Eq. (1). Therefore, it should be emphasized that the results shown in this study are for the average waveforms of the stimulus- and response-locked components and our method probes the average effects of the temporal overlapping.

The stimulus- and response-locked components are extracted by calculating the left-hand side of Eqs. (10) and (11), respectively. The

equations are obtained by solving Eqs. (2) and (3) simultaneously. On the other hand, we are able to define other sets of simultaneous equations to obtain the extracted stimulus- and response-locked components. For example, we are able to use the equation:

$$Y_{n'}(\omega) = S(\omega) + \exp(-i2\pi\omega\tau_{n'}/T)R(\omega) + V_{n'}(\omega) \tau_n \neq \tau_{n'}, \quad (17)$$

instead of Eq. (3). Like Eq. (3), Eq. (17) is different from Eq. (2) in that the RTs are different ($\tau_n \neq \tau_{n'}$), and we can solve Eqs. (2) and (17) for $s(t)$ and $r(t)$. However, in that case the denominator of the solved equations frequently tends to be zero, making the decomposition difficult. We also tried some other simultaneous equations instead of Eqs. (2) and (3). Among these trials, Eqs. (2) and (3) are the best in that the denominators of the solved equations rarely become zero, and the calculation for the decomposition is simple. Even if the denominators of Eqs. (10) and (11) do become zero, we have a solution: adjust $T (=I_0 + I_1)$ so that the denominator does not become zero.

We non-parametrically decomposed single-channel EEG into the stimulus- and response-locked components using a discrete Fourier transform. An alternative would be to identify parametric models of evoked potentials (for example, Cerutti et al., 1987; Jensen et al., 1996; Litvan et al., 2002). In our preliminary study, indeed, we were also able to identify these components parametrically using a Finite Impulse Response model. Another alternative would be applying Woldorff's method (1993), called the Adjacent Response (Adjar) technique. In the time domain, the Adjar removes the distortion due to the overlap of the consecutive event-related potentials in short inter-stimulus intervals. Although originally developed to extract only the stimulus-locked component, the Adjar could also be used to extract not only the stimulus-locked component but also the response-locked component (Braun et al., 2002). As far as comparable performance is obtained, we believe our method is better because it does not require a priori knowledge of parametric models themselves, and its rationale and procedure are quite simple and clear.

The simulation results show that the noise level of the components extracted by our method is larger than that of the stimulus-/response-triggered average. The amplitude spectra of the residual errors (Figs. 2B2, C2) indicate that this is because the absolute value of $1/D(n, \omega)$ is higher at low frequencies (~ 1 Hz) if the observed RTs are used as τ_n ; that is, slow waves (~ 1 Hz) in the noise are amplified by the decomposition. In other words, the larger noise in the extracted stimulus-/response-locked components is attributable to the decomposition itself rather than to the other data operations, such as the data segmentation strategy. On the other hand, the simulation results also show that the noise level of the extracted components decreases as the number of trials increases. These results lead to solutions for this methodological limitation: increasing the number of trials and/or applying a high-pass filter to the EEG before the decomposition. The number of trials required for each filter property is shown in Table 1.

Generally speaking, a higher cut-off frequency of the EEG leads to a smaller number of trials, but that would also result in the attenuation of slower potentials of interest, as in our case of the EEG filtered with 2–40 Hz (Fig. 8). To prevent this, employing a higher number of trials with minimally filtered EEG would be a choice, but the noise level for this is substantially greater than that for the simple averaging. The averaging procedure, then, is not capable of perfectly separating temporally overlapping components when a stimulus and a response are temporally closer, as shown in the

present study. Thus, one would need to balance one choice against the others, depending on the phenomenon of interest and practical limitations of the research settings.

Temporal smearing in averaged EEG

In this study, we examine the effect of the temporal smearing by comparing the extracted stimulus-/response-locked components with the stimulus-/response-triggered average EEG during the SR-task. Here, we quantitatively describe the level of the temporal smearing. Under the assumption of Eq. (1), the stimulus-triggered average EEG $\bar{y}_s(t)$ is expressed by:

$$\bar{y}_s(t) = s(t) + \frac{1}{N} \sum_{\tau=0}^t h(\tau)r(t-\tau) + \frac{1}{N} \sum_{n=1}^N v_n(t), \quad (18)$$

where $h(\tau)$ represents the distribution of RTs. In this equation, the temporal smearing by the response-locked component is expressed by $1/N \sum_{\tau=0}^t h(\tau)r(t-\tau)$. Similarly, the response-triggered average EEG $\bar{y}_r(t)$ is expressed by:

$$\bar{y}_r(t) = r(t) + \frac{1}{N} \sum_{t=0}^{T-t-1} h(\tau)s(t+\tau) + \frac{1}{N} \sum_{n=1}^N v_n(t+\tau_n), \quad (19)$$

and in this equation the temporal smearing by the stimulus-locked component is expressed by $1/N \sum_{\tau=0}^{T-t-1} h(\tau)s(t+\tau)$. Obviously, the terms for the temporal smearing include stimulus- and response-locked components, indicating that we need these components to examine the temporal smearing. In other words, whether the temporal smearing is large or small should be unclear without the decomposition.

From Eqs. (18) and (19), it is shown that $\bar{y}_s(t) - s(t)$ and $\bar{y}_r(t) - r(t)$ mainly represent the temporal smearing in the stimulus-triggered average EEG and the response-triggered average EEG, respectively. Therefore, the presented differences between the extracted stimulus-/response-locked components and the stimulus-/response-triggered average EEG should represent the temporal smearing by the response-/stimulus-locked components.

Stimulus-locked EEG component

We extract the stimulus-locked components by Eq. (10) from the EEG data during the SR-task. The extracted stimulus-locked components exhibit the N100, P200, P300 and N400. The existence of the N100 and P200 is in agreement with previous studies which have examined EEG during simple reaction time tasks (Falkenstein et al., 1993; Hohnsbein et al., 1991). In this study, we evaluate the effect of the temporal overlapping at the late peaks: the P300 and N400.

As for the P300, the scalp distributions between the extracted stimulus-locked components and the stimulus-triggered average EEG appear to be different in the case of the EEG filtered with 1–40 Hz. However, the effect of the temporal smearing by the response-locked components is not so large as to change the global scalp distributions (measured by the dp) significantly. The local difference between the stimulus-locked P300 and the stimulus-triggered average P300, the former showing more frontal topology, should be studied further.

On the contrary, at the N400, the significant difference of the scalp distributions between the extracted stimulus-locked components and the stimulus-triggered average EEG is observed.

As for the EEG filtered with 1–40 Hz, the N400 amplitudes in the extracted stimulus-locked components are large in the central

region. The validity of the central N400 in the extracted stimulus-locked components is supported by a previous study which reports a stimulus-locked, centro-parietal N400 during audio-visual cognitive tasks with responses (Cummings et al., 2006). The result that the AEP, which is thought to reflect only a stimulus-related brain process, also has a centrally distributed N400 could also be evidence supporting the validity of the N400 in the extracted stimulus-locked components.

The scalp distributions of the N400 in the extracted stimulus-locked components are different from those in the stimulus-triggered average EEG. However, when the extracted response-locked components are overlapped on the stimulus-locked components, the difference in the N400 between them disappears. This suggests that the difference is attributable to the overlapping of the response-locked components.

As for the EEG filtered with 2–40 Hz, the N400 appears at around Cz even in the stimulus-triggered average EEG in the same way as the extracted stimulus-locked components. This is likely because, in the case of the EEG filtered with 2–40 Hz, the response-locked components are attenuated by the high-pass filter, and the resultant small effect of the temporal smearing discloses the original N400 in the stimulus-triggered average EEG. Its scalp distributions are similar across subjects; the dot product between a subject's vector and the other subjects' average vector is calculated for each subject and compared with zero by the Wilcoxon signed-rank test ($dp=0.83\pm 0.20$, $p<0.05$). Then again, the N400 which appears in the EEG filtered with 2–40 Hz additionally confirms the existence of the N400 in the stimulus-locked components extracted from the EEG filtered with 1–40 Hz.

The above results indicate that the differences between the stimulus-locked components and the stimulus-triggered average EEG can be attributed to the temporal overlapping of the response-locked components, and the effects of the temporal overlapping are different between the filter properties used, because the waveforms of the overlapping components vary depending on the filter properties.

On the other hand, although the auditory stimuli are the same during the SR-task and the S-task, the waveforms of the late parts in the extracted stimulus-locked components and the AEP are different; the AEP does not exhibit the clear P300 in contrast to the stimulus-locked components (Fig. 5). This indicates that even the “pure” stimulus-related activity is modulated depending on whether the response is required or not. In another task requiring no motor responses, different P300 evoked by the same stimuli in different instructions have also been reported (Verleger and Berg, 1991). These results might reflect the context-dependent modulation of the stimulus-related EEG activity.

Response-locked EEG component

In many studies which examine movement-related potentials, slow components of averaged EEG have been discussed (for example, Jankelowitz and Colebatch, 2002; Neshige et al., 1988; Papa et al., 1991; Shibasaki et al., 1980). However, in this study, such slow components are cut by the high-pass filter of 1 or 2 Hz because of the methodological limitation (see the Methodological considerations subsection). Therefore, in the present study we cannot easily deal with classical slow components, such as the Bereitschaftspotential (Neshige et al., 1988; Shibasaki et al., 1980).

We extract the response-locked components by Eq. (11) from the EEG data during the SR-task. The extracted response-locked com-

ponents exhibit the three distinct peaks: the N-40, P160 and N500. The existence of these peaks is in agreement with a previous study which examined EEG during cued movements (Papa et al., 1991). In this study, we evaluate the effect of the temporal overlapping at the earlier peaks: the N-40 and P160.

In the EEG filtered with both 1–40 and 2–40 Hz, the scalp distributions of the N-40 and P160 in the extracted response-locked components are similar to those in the response-triggered average EEG during the SR-task. This suggests that the distributions of the response-locked components are less smeared by the temporal overlapping of the stimulus-locked components. This is because the stimulus-locked components do not have large slow waves in comparison with the response-locked components and, by the averaging procedure, are easily diminished as a result of phase cancellations of fast waves.

The MRP do not exhibit the clear N-40, in contrast to the response-locked components and the response-triggered average EEG. By the averaging procedure, some studies (Jankelowitz and Colebatch, 2002; Papa et al., 1991) have also revealed different EEG activity during self-paced movements and cued movements. The similarity of the response-locked component and the response-triggered average EEG allows us to suggest that the differences in the response-triggered average EEG between the tasks observed in this and previous studies are due not to the temporal overlapping of the stimulus-locked components but to the context-dependent modulation of response-related EEG activity.

Although the subjects responded with their right index fingers, significant asymmetry is not observed for the N-40 and P160 in the extracted response-locked components, in contrast to the response-triggered average EEG and to previous studies (for example, by Neshige et al., 1988). This is because the noise amplified by the decomposition makes the inter-subject variability of the N-40 and P160 distributions large and the p -values become higher.

Conclusion

In conclusion, the results presented in this paper confirm the feasibility and usefulness of the frequency domain decomposition of EEG data into stimulus- and response-locked components during a reaction time task, and show that the contamination by the temporal overlapping is large especially in the late part of the stimulus-triggered average EEG during the SR-task when slow waves remain in the EEG data.

It should be noted that the effect of the temporal smearing shown in this study may not hold true for every reaction time task. This is because the effect of the temporal smearing is determined by the distribution of RTs and the waveform of the stimulus- or response-locked components [see Eqs. (18) and (19)]; that is, the contamination is task-dependent and cannot be examined directly without the decomposition. Therefore, to examine the brain activity during reaction time tasks in detail, the decomposition is required eventually, regardless of which components we use and whether they are obtained by the averaging procedure or by our method.

References

- Braun, C.M.J., Villeneuve, L., Gruzelier, J.H., 2002. Topographical analysis of stimulus-related and response-related electrical scalp activity and interhemispheric dynamics in normal humans. *Int. J. Psychophysiol.* 46, 109–122.
- Cerutti, S., Baselli, G., Liberati, D., Pavesi, G., 1987. Single sweep analysis

- of visual evoked potentials through a model of parametric identification. *Biol. Cybern.* 56, 111–120.
- Cummings, A., Čeponienė, R., Koyama, A., Saygin, A.P., Townsend, J., Dick, F., 2006. Auditory semantic networks for words and natural sounds. *Brain Res.* 1115, 92–107.
- Endo, H., Kizuka, T., Masuda, T., Takeda, T., 1999. Automatic activation in the human primary motor cortex synchronized with movement preparation. *Cogn. Brain Res.* 3, 229–239.
- Falkenstein, M., Hohnsbein, J., Hoormann, J., 1993. Late visual and auditory ERP components and choice reaction time. *Biol. Psychol.* 35, 201–224.
- Gibbons, H., Stahl, J., 2007. Response-time corrected averaging of event-related potentials. *Clin. Neurophysiol.* 118, 197–208.
- Goodin, D.S., Aminoff, M.J., Mantle, M.M., 1986. Subclasses of event-related potentials: response-locked and stimulus-locked components. *Ann. Neurol.* 20, 603–609.
- Hohnsbein, J., Falkenstein, M., Hoormann, J., Blanke, L., 1991. Effects of crossmodal divided attention on late ERP components: I. Simple and choice reaction tasks. *Electroencephalogr. Clin. Neurophysiol.* 78, 438–446.
- Jankelowitz, S.K., Colebatch, J.G., 2002. Movement-related potentials associated with self-paced, cued and imagined arm movements. *Exp. Brain Res.* 147, 98–107.
- Jensen, E.W., Lindholm, P., Henneberg, S.W., 1996. Autoregressive modeling with exogenous input of middle-latency auditory-evoked potentials to measure rapid changes in depth of anesthesia. *Methods Inf. Med.* 35, 256–260.
- Jung, T.-P., Makeig, S., Westerfield, M., Townsend, J., Courchesne, E., Sejnowski, T.J., 2001. Analysis and visualization of single-trial event-related potentials. *Hum. Brain Mapp.* 14, 166–185.
- Lamarre, Y., Busby, L., Spidalieri, G., 1983. Fast ballistic arm movements triggered by visual, auditory, and somesthetic stimuli in the monkey: I. Activity of precentral cortical neurons. *J. Neurophysiol.* 50, 1343–1358.
- Litvan, H., Jensen, E.W., Galan, J., Lund, J., Rodriguez, B.E., Henneberg, S.W., Caminal, P., Villar Landeira, J.M., 2002. Comparison of conventional averaged and rapid averaged, autoregressive-based extracted auditory evoked potentials for monitoring the hypnotic level during propofol induction. *Anesthesiology* 97, 351–358.
- Mihaylova, M., Stomonyakov, V., Vassilev, A., 1999. Peripheral and central delay in processing high spatial frequencies: reaction time and VEP latency studies. *Vis. Res.* 39, 699–705.
- Nelson, R.J., 1987. Activity of monkey primary somatosensory cortical neurons changes prior to active movement. *Brain Res.* 406, 402–407.
- Nelson, R.J., Smith, B.N., Douglas, V.D., 1991. Relationships between sensory responsiveness and premovement activity of quickly adapting neurons in areas 3b and 1 of monkey primary somatosensory cortex. *Exp. Brain Res.* 84, 75–90.
- Neshige, R., Lüders, H., Shibasaki, H., 1988. Recording of movement-related potentials from scalp and cortex in man. *Brain* 111, 719–736.
- Papa, S.M., Artieda, J., Obeso, J.A., 1991. Cortical activity preceding self-initiated and externally triggered voluntary movement. *Mov. Disord.* 6, 217–224.
- Perfilev, S.N., 1998. Responses in the motor cortex time-locked to the sensory stimuli conditioning target-reaching in the cat. *Neurosci. Res.* 32, 273–279.
- Shibasaki, H., Barrett, G., Halliday, E., Halliday, A.M., 1980. Components of the movement-related cortical potential and their scalp topography. *Electroencephalogr. Clin. Neurophysiol.* 111, 719–736.
- Tanji, J., Kurata, K., 1982. Comparison of movement-related activity in two cortical motor areas of primates. *J. Neurophysiol.* 48, 633–653.
- Thompson, K.G., Hanes, D.P., Bichot, N.P., Schall, J.D., 1996. Perceptual and motor processing stages identified in the activity of macaque frontal eye field neurons during visual search. *J. Neurophysiol.* 76, 4040–4055.
- Vassilev, A., Mihaylova, M., Bonnet, C., 2002. On the delay in processing high spatial frequency visual information: reaction time and VEP latency study of the effect of local intensity of stimulation. *Vis. Res.* 42, 851–864.
- Vaughan Jr., H.G., Costa, L.D., Gilden, L., 1966. The functional relation of visual evoked response and reaction time to stimulus intensity. *Vis. Res.* 6, 645–656.
- Verleger, R., Berg, P., 1991. The waltzing oddball. *Psychophysiology* 28, 468–477.
- Woldorff, M.G., 1993. Distortion of ERP averages due to overlap from temporally adjacent ERPs: analysis and correction. *Psychophysiology* 30, 98–119.